Distributed Control of Large-Scale Inverter Air Conditioners for Providing Operating Reserve Based on Consensus With Nonlinear Protocol

Jiatu Hong, *Student Member, IEEE*, Hongxun Hui, *Member, IEEE*, Hongcai Zhang, *Member, IEEE*, Ningyi Dai, *Senior Member, IEEE*, and Yonghua Song, *Fellow, IEEE*

***Abstract*—Rapidly increasing renewable energies bring more fluctuations to the power system and put forward higher requirement on operating reserve for maintaining the system balance. Traditional generating units are phasing out and may be insufficient to satisfy this reserve requirement in the near future. Therefore, much attention is paid to demand-side regulation resources. Inverter air conditioners (IACs) account for about 30% of the total power consumption in cities and have huge regulation potential. However, the control of large-scale dispersed IACs is intractable. Most existing studies adopt the centralized control scheme to regulate IACs, while it requires a high-cost communication infrastructure and induces privacy concerns. To address this issue, this article investigates the distributed control scheme of large-scale dispersed IACs for providing operating reserve. First, a normalization approach is proposed to uniformly quantify the regulation capacities of heterogeneous IACs. Then, a distributed consensus algorithm with a nonlinear protocol is developed for IACs to achieve the regulation objective under guaranteeing customers' comfort requirements. Based on the Lyapunov stability theorem, the convergence of the proposed algorithm on large-scale dispersed IACs is proved to be always guaranteed. Finally, numerical studies verify the feasibility and performance of the proposed method, which features better data privacy protection and less communication and computation burden than the centralized control methods.**

***Index Terms*—Distributed control, inverter air conditioner (IAC), Lyapunov stability, nonlinear consensus, operating reserve.**

NOMENCLATURE

Abbreviation

ACs	Air conditioners.
COP	Coefficient of performance.
DR	Demand Response.
ETP	Equivalent thermal parameters.
GW	Gigawatt.
IACs	Inverter air conditioners.
MW	Megawatt.
RENs	Renewable energies.

Set

$\mathcal{E}$	Set of edges for a graph.
$\mathcal{V}$	Set of vertices for a graph.
$\mathcal{I}$	Set of IACs.
$\mathcal{N}_i$	Set of all the ith IAC's neighbors.
$\mathcal{T}$	Set of time slots.

Parameter

β	Control coefficient of relay nodes.
$\boldsymbol{A}$	Adjacency matrix.
$\boldsymbol{D}$	Degree matrix.
$\boldsymbol{L}$	Laplacian matrix.
$\Delta T_{\max}$	Allowable temperature deviation range.
λ	Decision value after the system convergence.
$\overline{f_i}$	Upper limitation of the ith IAC's operating frequency.
$\underline{f_i}$	Lower limitation of the ith IAC's operating frequency.
a_{ij}	Element of adjacency matrix.
b_{i1}	Coefficient of the ith IAC's operating power.
b_{i2}	Coefficient of the ith IAC's cooling capacity.
c	Control gain.
C_i	Equivalent air heat capacity of the ith room.
d_i	ith diagonal element of the degree matrix.
f_i^0	Initial operating frequency of the ith IAC.
l_{i1}	Coefficient of the ith IAC's operating power.
l_{i2}	Coefficient of the ith IAC's cooling capacity.
N	Total number of nodes in the communication network.
P_{tgt}	Regulation capacity target instructed by the aggregator.
R_i	Equivalent thermal resistance of the ith room's envelope.
s	Laplace operator.
$T^i_{\max}$	Upper bound of comfort range.
$T^i_{\min}$	Lower bound of comfort range.
T^i_{set0}	Initial set temperature.

Variable

$\bar{y}$	Initial average value of y_i.
COP_i	Coefficient of performance for the ith IAC.

Manuscript received 14 September 2021; revised 13 January 2022; accepted 6 February 2022. Date of publication 16 February 2022; date of current version 24 August 2022. This work was supported by the Science and Technology Development Fund, Macau, under Grant SKL-IOTSC(UM)-2021-2023 and Grant 0003/2020/AKP. *(Corresponding author: Hongxun Hui.)*

The authors are with the State Key Laboratory of Internet of Things for Smart City and the Department of Electrical and Computer Engineering, University of Macau, Macau, China (e-mail: jiatu.hong@connect.um.edu.mo; hongxunhui@um.edu.mo; hczhang@um.edu.mo; nydai@um.edu.mo; yhsong@um.edu.mo).

Digital Object Identifier 10.1109/JIOT.2022.3151817

f_i	Operating frequency of the ith IAC.
P_i	Operating power of the ith IAC.
P_{DR}	Total regulation capacity value in real time.
Q_i	Cooling capacity of the ith IAC.
x_i	State of the ith IAC.
T_i	Indoor air temperature of the ith room.
T_o	Outdoor temperature.
V	Lyapunov function.
r_i	State of the ith relay node.
y_i	Intermediate variable in control diagram of ith IAC.

I. Introduction

RENEWABLE energies (RENs), such as photovoltaic and wind generators, are booming in power systems across the world. For example, more than 260-GW RENs are installed globally in 2020, despite the COVID-19 pandemic [1]. However, RENs bring more fluctuating power and put forward higher requirement on the operating reserve for maintaining the power system balance [2]. Generally, the operating reserve is the generating capacity available to the system operator within a short interval of time to deal with fluctuating or contingency conditions [3]. With the phasing out of traditional generating units (e.g., thermal generators), the operating reserve may be further insufficient in the near future. Therefore, exploring more flexible regulation resources to provide operating reserve becomes a worldwide hotspot [4].

The progressed Internet of Things technologies make it easier to control massive flexible loads as regulation resources [5], which is named DR [6]. Among different flexible loads, ACs are one of the most promising regulation candidates [7], [8]. Generally, ACs can be divided into two categories, i.e., traditional fixed-frequency ACs and IACs [9]. The main difference lies in the compressor. The fixed-frequency AC's compressor operates in two modes (i.e., ON and OFF) to adjust the indoor temperature [10]. In contrast, the IAC's compressor operates with variable speed and can be adjusted more flexibly by the inbuilt inverter [11]. Hence, IACs are more suitable to be regulated to provide operating reserve for power systems. There are mainly three reasons that we specifically pay attention to IACs for providing ancillary services. First, ACs account for about 60% of the total power consumption in cities during summer peak hours [12]. Among different types of ACs, IACs are equipped with advanced power electronic technologies and gradually dominate the ACs' market due to advantages in efficiency and comfort [13]. Second, the thermal inertia of buildings serves as the foundation for ACs participating in DR [14]. The comfort of customers can be guaranteed when the power consumption of ACs (including IACs) is temporarily decreased/increased. Third, the residential density of cities is pretty high. The distance between two neighboring IACs is short. Hence, the communication network among IACs can be built by wireless way, which is more convenient and low cost for the implementation of distributed control on IACs [15].

In addition, the regulation service provided by aggregated IACs is defined from the following three perspectives: 1) regulation capacity; 2) regulation speed; and 3) duration time.

1) For aggregated IACs providing operating reserve, the *regulation capacity* denotes how much power can be decreased in the upregulation scenario (or increased in the downregulation scenario).
2) Generally, the system operator is concerned whether the regulation capacity can be achieved in a timely manner. When the aggregator receives the dispatch signal from the system operator, it sends control signals to IACs for power regulation. The *regulation speed* denotes how fast the aggregated IACs can reach the target regulation capacity. In realistic power systems around the world, the operating reserve generally should be provided within 10 min [16].
3) The power regulation on IACs would inevitably influence the corresponding rooms' indoor temperatures. It means that the regulation process cannot last an arbitrary long time compared with traditional generators. Hence, the *duration time* denotes the period from the beginning of providing operating reserve to the end of the regulation process.

In most literature, the centralized control method is adopted to regulate large-scale IACs for participating in DR, where the control center is generally regarded as an aggregator to be responsible for controlling a vast number of IACs [17]. The aggregator exchanges information with each individual IAC based on the bidirectional communication channel, including uplink available regulation capacities and downlink control signals [18]. Normally, thousands of IACs are aggregated to provide significant regulation capacity, which leads to high investment in the real-time communication infrastructure in the centralized control method. In contrast, the distributed control method does not require vast communication between the aggregator and massive terminal devices [19]. For example, Zeraati *et al.* [20] proposed a distributed control method to regulate batteries for solving the voltage fluctuations brought by photovoltaic generators, which is based on distributed local controllers. Ding *et al.* [21] proposed a distributed control method to regulate ACs for utilizing RENs, which shows the aggregator's computation burden can be relieved greatly. Hence, the distributed control method is probably an alternative solution to control IACs for providing operating reserve [22]. However, there are several difficulties to control large-scale IACs in real time, mainly in the following *three aspects*.

1) *Satisfying the System's Regulation Requirement:* The regulation requirement of the operating reserve generally includes the regulation capacity (i.e., the total decrease/increase power of IACs) and the response time (i.e., from the control signal sending time to the IACs' action time) [23]. In the distributed control method, massive IACs take action autonomously, which makes it difficult to guarantee the response speed and the control accuracy of aggregated IACs' regulation capacity.
2) *Guaranteeing Heterogeneous Customers' Comfort:* All the indoor temperature should be maintained within the customers' desired comfortable ranges when the IACs are controlled to provide operating reserve [24].

However, the IAC's COP, real-time outdoor temperature, corresponding building's heat capacity, and thermal resistance are variable and uncertain, which may affect the indoor temperature to exceed the comfortable ranges during the regulation process.

3) *Ensuring the Control Convergence:* During the regulation process, some IACs may withdraw the regulation and stop providing operating reserve due to the customers' instructions or violations of comfortable indoor temperature. In other words, the IACs' participating number and the distributed communication network may change with time, which makes it intractable to ensure the distributed control method's convergence (i.e., fulfil the overall regulation requirement of aggregated IACs) in uncertain changeable conditions [25].

To address the above issues, some studies propose to use the consensus algorithm (a distributed control method via local neighboring interactions) to control large-scale flexible resources [26], [27]. The distributed consensus algorithm has attracted a lot of research interests in recent years [28]. Mo and Murray [29] proposed a privacy-preserving average consensus algorithm by adding and subtracting random noises to the consensus process to protect the privacy of the initial state. Chen *et al.* [30] introduced the consensus algorithm in the microgrid application scenarios, which focuses on the improvement of the communication strategy through the event-triggered control mechanism. Fu *et al.* [31] investigated the consensus problem for multiagent systems with input saturation, which considers the limited actuation power of physical plants. In addition, Bhowmick and Panja [32] proposed a bipartite consensus method to deal with two antagonistic groups in specific application scenarios, in which two groups in the network can reach respective decision values.

In respect to the application of the consensus algorithm for DR, Wang *et al.* [33] developed a consensus control strategy for IACs to realize the fair allocation of regulation power. Xing *et al.* [34] proposed a consensus problem to achieve the fast convergence of IACs under a limited local communication network. Wang *et al.* [35] designed a consensus algorithm for IACs in building-microgrid community to improve the local utilization rate of solar generation. However, these studies do not consider IACs' heterogeneous physical constraints and application scenario requirements, which may cause the customers' discomfort and response failure. Furthermore, to the best of our knowledge, the withdrawal process of IACs during the regulation process has not been considered previously, which may lead to the insufficiency of the actual operating reserve and threaten the secure operation of the power system. To deal with these problems, this article proposes a novel distributed control method of large-scale dispersed IACs based on the consensus algorithm with a nonlinear protocol. The main contributions are summarized as follows.

1) A normalization approach is proposed to uniformly quantify the regulation capacity of heterogeneous IACs. On this basis, a distributed consensus algorithm with the nonlinear protocol is developed to control IACs for achieving the regulation objective under different physical constraints and application scenario requirements.

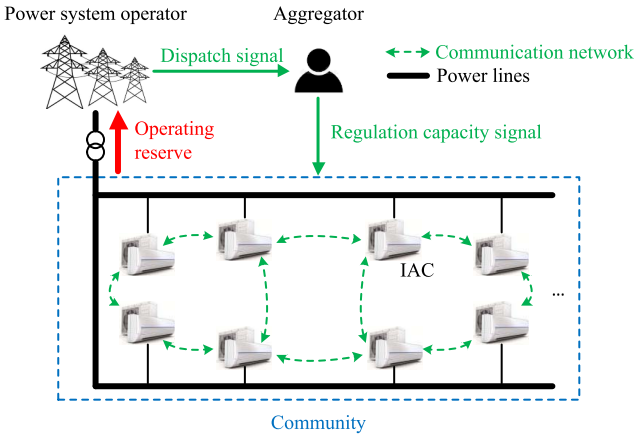

Fig. 1. Control framework of large-scale dispersed IACs for providing operating reserve in the power system.

2) To guarantee different customers' comfort requirements, a smooth withdrawal mechanism is proposed to terminate the regulation process of IACs violating their comfort constraints. This withdrawal mechanism can sustain the total required operating reserve by compensating the lost regulation capacity from the remaining available IACs.
3) Based on the Lyapunov stability theorem, the convergence of the proposed consensus algorithm is proved considering different physical characteristics of large-scale IACs and heterogeneous customers' requirements on the indoor temperature.

The remainder of this article is organized as follows. First, preliminaries about the control framework and basic theory are introduced in Section II. The proposed consensus algorithm with the nonlinear protocol is presented in Section III. Section IV illustrates numerical studies. Section V concludes this article.

II. Preliminaries

A. Control Framework of IACs

To maintain the real-time power balance between the supply side and demand side, the power system operator will send dispatch signals to DR providers to obtain operating reserve when traditional generating units are insufficient. In this article, DR providers refer to IACs, as shown in Fig. 1.

Generally, one IAC's regulation capacity is too small to directly interact with the power system operator. Large-scale IACs are aggregated by the aggregator to provide significant operating reserve for the power system. Therefore, the aggregator is responsible for communicating and controlling a vast number of IACs to meet the requirement from the system operator, which is exactly the focus of this article. The consensus algorithm is adopted in Fig. 1, where most IACs only communicate with their neighbors instead of communicating with the aggregator. Compared with traditional centralized control methods, the signal transmission network between the aggregator and massive IACs can be greatly simplified. Moreover, the distributed control method framework also contributes to the privacy protection, because the

customers' power consumption data does not need to be transmitted to the aggregator. The proposed consensus algorithm will be illustrated in detail in Section III.

B. Thermodynamic Model of IACs

Since the comfortable indoor temperature is customers' major concern when they participate in DR, the IAC's operation model and the corresponding room's thermodynamic model need to be developed. Based on the first-order ETP model [36], the thermodynamic process of the room can be expressed as

$$C_i \frac{dT_i(t)}{dt} = \frac{T_o(t) - T_i(t)}{R_i} - Q_i(t) \quad \forall i \in \mathcal{I} \quad \forall t \in \mathcal{T} \quad (1)$$

where C_i is the equivalent air heat capacity of the ith room; R_i is the equivalent thermal resistance of the ith room's envelope; $T_i(t)$ is the ith room's indoor air temperature at time t; $T_o(t)$ is the outdoor temperature at time t; $Q_i(t)$ is the cooling capacity of the ith IAC at time t; and $\mathcal{I}$ and $\mathcal{T}$ are sets of IACs and time slots, respectively.

The compressor accounts for the majority of one IAC's energy consumption, because it provides the cooling capacity for the room. Based on the realistic test data [37], the IAC's operating power and corresponding cooling capacity can be simplified as linear with its compressor's operating frequency, which is expressed as

$$P_i(t) = l_{i1} f_i(t) + b_{i1} \quad \forall i \in \mathcal{I} \quad \forall t \in \mathcal{T} \quad (2)$$

where $P_i(t)$ and $f_i(t)$ are the ith IAC's operating power and compressor's operating frequency at time t, respectively. Both l_{i1} and b_{i1} are the coefficients of the ith IAC's operating power. Similarly, the cooling capacity of the IAC can be expressed as

$$Q_i(t) = l_{i2} f_i(t) + b_{i2} \quad \forall i \in \mathcal{I} \quad \forall t \in \mathcal{T} \quad (3)$$

where $Q_i(t)$ is the ith IAC's cooling capacity at time t. Both l_{i2} and b_{i2} are the coefficients of the ith IAC's cooling capacity. Based on (2) and (3), the electrothermal conversion relation of the ith IAC can be derived as

$$Q_i(t) = \frac{l_{i2}}{l_{i1}} P_i(t) + \frac{l_{i1} b_{i2} - l_{i2} b_{i1}}{l_{i1}} \quad \forall i \in \mathcal{I} \quad \forall t \in \mathcal{T}. \quad (4)$$

According to (1) and (4), the relationship between the indoor temperature and IAC's power consumption is established. Note that the thermostatically controlled load's COP is defined as $\mathrm{COP}_i(t) = Q_i(t)/P_i(t)$, which is variable with time for IACs. This is one of the major different characteristics compared with traditional fixed-frequency ACs, whose COP_i is generally regarded as a fixed value. The variable $\mathrm{COP}_i(t)$ exacerbates the difficulty of controlling IACs to provide the required operating reserve and maintain comfortable indoor temperature at the same time.

C. Basic Graph Theory

The basic graph theory serves as the fundamental of the distributed consensus control method. The graph $\mathcal{G} = (\mathcal{V}, \mathcal{E})$ features with the set of vertices $\mathcal{V} = \{v_1, v_2, \ldots, v_N\}$ and the set of edges $\mathcal{E} \subseteq \mathcal{V} \times \mathcal{V}$. In this article, $\mathcal{V}$ indicates the set of IACs and $\mathcal{E}$ indicates the communication relationship among IACs. In addition, graph $\mathcal{G}$ is considered as undirected, i.e., bidirectional communication exists between two neighbor IACs. The corresponding adjacency matrix $\boldsymbol{A} = [a_{ij}]$ of graph $\mathcal{G}$ with 0–1 weights is defined as

$$a_{ij} = \begin{cases} 1, & \forall (v_i, v_j) \in \mathcal{E} \\ 0, & \text{otherwise.} \end{cases} \quad (5)$$

The corresponding Laplacian matrix $\boldsymbol{L}$ of graph $\mathcal{G}$ is defined and calculated by

$$\boldsymbol{L} = \boldsymbol{D} - \boldsymbol{A} \quad (6)$$

where $\boldsymbol{D}$ is the degree matrix and defined as $\boldsymbol{D} = \mathrm{diag}(d_1, d_2, \ldots, d_N)$ with $d_i = \sum_{j \neq i} a_{ij}$.

For the undirected graph $\mathcal{G}$, the Laplacian matrix $\boldsymbol{L}$ is symmetric with trivial zero eigenvalue corresponding to the eigenvector $\mathbf{1}$, and holds the following property [38]:

$$\boldsymbol{x}^T \boldsymbol{L} \boldsymbol{x} = \frac{1}{2} \sum_{(v_i, v_j) \in \mathcal{E}} a_{ij} (x_i - x_j)^2 \quad (7)$$

where $\boldsymbol{x} = [x_1, x_2, \ldots, x_N]^T$ indicates the states of vertices. Equation (7) reflects the agreement level among nodes (i.e., IACs) in the network. At the early stage of the regulation process, states (i.e., x_i and x_j) are different and exchanged with neighbors based on the consensus algorithm. When IACs in the network reach an agreement (i.e., the states converge), the value of (7) equals 0. In addition, the Laplacian matrix $\boldsymbol{L}$ is positive semidefinite since $\boldsymbol{x}^T \boldsymbol{L} \boldsymbol{x} \geq 0$ is guaranteed, which serves as a precondition for the convergence of the standard consensus algorithm introduced in Section III.

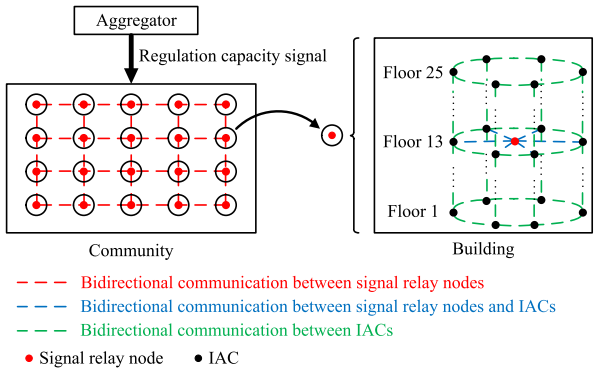

Fig. 2. Communication network of large-scale IACs in a community for providing operating reserve in the power system.

III. Consensus Control With Nonlinear Protocol

A. Communication Network of IACs

The communication network of IACs in a community is shown in Fig. 2. The community is assumed to have multiple high-rise buildings. For example, Fig. 2 shows a community with 20 buildings. In each building, there are 25 floors with six rooms on each floor.[1] There are three kinds of communication channels. First, in order to realize the communication between

[1]It is assumed that each room has one IAC, which is equipped with a control module for the communication and control purpose.

the aggregator and each building, one signal relay node is assigned for each building (i.e., the red node). Relay nodes are also interconnected with nearby buildings' relay nodes (i.e., the red-dotted lines) to improve the system reliability when facing the communication faults between the aggregator and some relay nodes.[2] Second, after receiving regulation signals from the aggregator or other relay nodes, the signal relay nodes will communicate with nearby IACs inside the buildings (i.e., the blue dotted lines). Third, all the IACs communicate bidirectionally with their neighbors in real time, including the left, right, upper, and lower neighbors (i.e., the green dotted lines).

In this article, the regulation requirement from the power system operator is assumed to be the decrease/increase value of IACs' operating power and corresponding beginning/ending response time. The aggregator is responsible for controlling the IACs in the community to fulfill this requirement. For example, the dispatch signal is sent to the aggregator at 12:00 A.M. to decrease IACs' operating power of 2 MW in the next 15 min. Then, the aggregator sends this requirement to relay nodes, and relay nodes further communicate with nearby IACs. In the next 15 min, IACs will communicate bidirectionally with their neighbors to coordinate and provide the required regulation capacity.

There are mainly three objectives during the control process of IACs: 1) achieve the total regulation requirement instructed by the aggregator; 2) achieve a similar utilization level of different IACs' regulation capacities to avoid heavy impact on specific IACs; and 3) guarantee all the rooms' indoor temperatures within customers' desired comfortable ranges.

The consensus algorithm with the nonlinear protocol is introduced as the main control methodology in this article for achieving the above objectives. The implementation steps are as follows: first, the states of vertices (i.e., IACs) $\boldsymbol{x} = [x_1, x_2, \ldots, x_N]^T$ in the graph $\mathcal{G} = (\mathcal{V}, \mathcal{E})$ need to be defined for regulating the IACs' operating power (the first control objective). Then, the consensus algorithm during the regulation process should be developed to share the impacts on IACs (the second control objective). Next, the withdrawal mechanism of IACs should be designed to guarantee heterogeneous comfort requirements of customers (the third control objective). Furthermore, the convergence of the proposed algorithm needs to be proved. These four steps will be illustrated specifically in the following sections.

B. State Definition of IACs

To achieve the distributed control of large-scale IACs based on the consensus algorithm, the information exchanged between neighbor interconnected IACs, i.e., vertices' states $\boldsymbol{x} = [x_1, x_2, \ldots, x_N]^T$, are defined as

$$x_i(t) = \begin{cases} \frac{f_i(t) - f_i^0}{\underline{f_i} - f_i^0} & \forall i \in \mathcal{I} \quad \forall t \in \mathcal{T}, \quad \text{Up regulation} \\ \frac{f_i(t) - f_i^0}{\overline{f_i} - f_i^0} & \forall i \in \mathcal{I} \quad \forall t \in \mathcal{T}, \quad \text{Down regulation} \end{cases} \tag{8}$$

where $f_i(t)$ is the operating frequency of the ith IAC's compressor at time t; f_i^0 is the initial operating frequency of the ith IAC's compressor at the beginning of regulation; $\underline{f_i}$ is the inherent lower limitation of the ith IAC's operating frequency subject to device characteristics; and $\overline{f_i}$ is the upper limitation of the ith IAC's operating frequency. The main difference between the up and downregulation scenarios is that the upregulation scenario is to increase the power system frequency by decreasing the IACs' operating power. In contrast, the downregulation is to decrease the power system frequency by increasing the IACs' operating power. During each round of dispatch, the power system operator sends control signals to the aggregator, which include the information about up or downregulation services. The information exchange among IACs also includes a binary option instruction about the up or downregulation services. In this manner, the IACs' controllers can choose the calculation rules in (8). Therefore, IACs only transmit the states $\boldsymbol{x}$. The exact operating information (f_i^0 and f_i) and physical features ($\underline{f_i}$ and $\overline{f_i}$) are concealed to each other, so that the customers' data privacy can be better protected.

According to (2), the IAC's power consumption is regarded as linear with the operating frequency. The denominators of (8) can denote the maximum regulation range of the ith IAC's operating frequency. Hence, the defined IACs' states $\boldsymbol{x}$ essentially indicates the utilization level of their maximum power regulation potential, which is the fundamental to achieve the control objective 2) mentioned in Section III-A. The states $\boldsymbol{x}$ are subject to IAC's physical constraints and application scenario requirements by

$$x_i(t) \in [0, 1] \quad \forall i \in \mathcal{I} \quad \forall t \in \mathcal{T}. \tag{9}$$

Take the upregulation scenario for example, the upper bound 1 denotes that the ith IAC's minimum operating frequency is $\underline{f_i}$. The lower bound 0 denotes that the ith IAC cannot operate with the frequency higher than f_i^0 during the upregulation process. To sum up, heterogeneous IACs' power regulation capacities are normalized as the utilization level ranging from 0 to 1 in (8) and (9), which is the important foundation for implementing the consensus algorithm.

C. Nonlinear Consensus Algorithm of IACs

The standard average consensus algorithm for the undirected graph can be expressed as

$$\dot{x}_i(t) = \sum_{j \in \mathcal{N}_i} a_{ij}\big(x_j(t) - x_i(t)\big) \quad \forall i \in \mathcal{I} \quad \forall t \in \mathcal{T} \tag{10}$$

where $\mathcal{N}_i$ is the set of all the ith IAC's neighbors; a_{ij} is the element of the adjacency matrix $\boldsymbol{A}$; and x_i and x_j are the defined states of the ith and jth IACs in (8), respectively. The corresponding matrix form of (10) can be expressed as

$$\dot{\boldsymbol{x}} = \boldsymbol{u} = -\boldsymbol{L}\boldsymbol{x} \tag{11}$$

where the Laplacian matrix $\boldsymbol{L}$ plays a feedback role [38]. Then, we can obtain the diagram of the standard average consensus algorithm, as shown in Fig. 3.

According to (7), the Laplacian matrix $\boldsymbol{L}$ is positive semidefinite and the algorithm in (11) is essentially the gradient-descent algorithm

$$\dot{\boldsymbol{x}} = -\nabla\big(\boldsymbol{x}^T\boldsymbol{L}\boldsymbol{x}\big)/2. \tag{12}$$

[2]Signal relay nodes only play the role as communication medium between the aggregator and IACs, while do not provide regulation capacities.

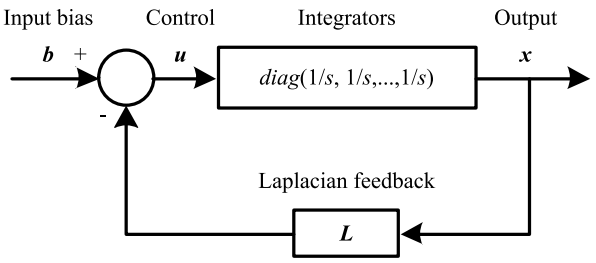

Fig. 3. Diagram of the standard average consensus algorithm.

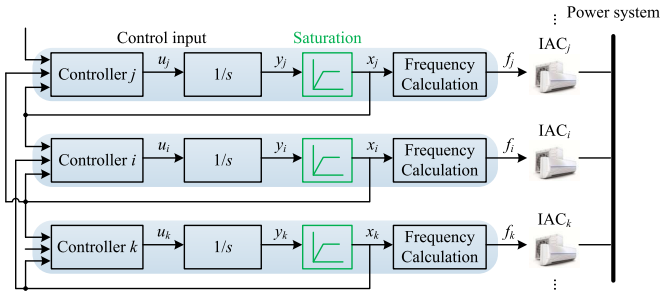

Fig. 4. Control diagram of large-scale dispersed IACs based on the nonlinear consensus algorithm.

According to the definition of the IAC's state in (8) and (9), the nonlinear saturation effect needs to be incorporated into the control of IACs. The standard consensus algorithm in (10) is transformed into the following form as:

$$x_i(t) = \text{sat}\big[y_i(t)\big] \quad \forall i \in \mathcal{I} \quad \forall t \in \mathcal{T} \tag{13}$$

$$\dot{y}_i(t) = c \sum_{j \in \mathcal{N}_i} a_{ij}\big(x_j(t) - x_i(t)\big) \tag{14}$$

where $y_i(t)$ is the intermediate variable; c is the control gain; and sat$(\cdot)$ denotes the nonlinear saturation function as follows:

$$\text{sat}\big[y_i(t)\big] = \begin{cases} 0, & y_i(t) < 0 \\ y_i(t), & 0 \le y_i(t) \le 1 \\ 1, & y_i(t) > 1. \end{cases} \tag{15}$$

From (13)–(15), the matrix form of the consensus algorithm with the nonlinear protocol can be expressed as

$$\dot{\boldsymbol{y}} = -c\boldsymbol{L}\boldsymbol{x} \tag{16}$$

where $\boldsymbol{x} = [\text{sat}(y_1), \text{sat}(y_2), \ldots, \text{sat}(y_N)]^T$. On this basis, the control diagram of IACs with the nonlinear saturation effect can be obtained, as shown in Fig. 4.

The ith IAC exchanges its state with two neighbor IACs and regulates its power consumption. Compared with the standard average consensus algorithm, the proposed control diagram in Fig. 4 incorporates a nonlinear saturation module to consider IACs' physical constraints and application scenario requirements. As for the upper saturation value "1," if there is no nonlinear saturation function, the control module may send the signal, which is even lower than the minimum operating frequency in the upregulation scenario (or the control module may send the signal which is even larger than the maximum operating frequency in the downregulation scenario). This is not applicable for the operation of real-world IACs. As for the lower saturation value "0," if there is no nonlinear saturation function, the control module may send the signal, which is even larger than the initial operating frequency in the upregulation scenario (or the control module may send the signal which is even lower than the initial operating frequency in the downregulation scenario), this is not acceptable for providing the required regulation services.

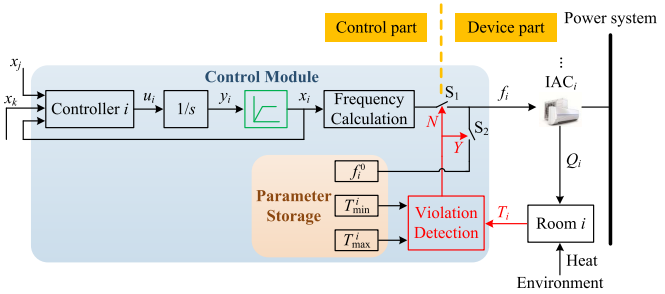

Fig. 5. Withdrawal mechanism of IACs for guaranteeing heterogeneous customers' comfort requirements.

Apart from IACs, the dynamics of relay nodes' states should also be derived, because relay nodes take the role as the communication medium between the aggregator and IACs. The states of relay nodes can be updated based on

$$\dot{r}_i(t) = c \sum_{j \in \mathcal{N}_i} a_{ij}\big(x_j(t) - r_i(t)\big) + \beta\big(P_{\text{tgt}} - P_{\text{DR}}(t)\big) \quad \forall i \in \mathcal{I} \quad \forall t \in \mathcal{T} \tag{17}$$

where $r_i(t)$ is the state of the ith relay node at time t; β is the control coefficient of relay nodes; P_{tgt} is the regulation capacity target instructed by the aggregator; and $P_{\text{DR}}(t)$ is the total regulation capacity value in real time, which can be monitored by the smart meter installed for the total power of IACs.

D. Withdrawal Method for Guarantee of Temperature Comfort

The power consumption of IACs is adjusted to provide operating reserve, which can impact the corresponding rooms' indoor temperature. Compared with the instant regulation of electric power, the indoor temperature relatively changes slowly due to the thermal inertia of buildings. However, when the regulation time is long or the regulation capacity is large, the indoor temperature may gradually exceed the comfort limitations set by customers. At this moment, the corresponding IACs need to immediately withdraw from the regulation process and recover the indoor temperature back to the comfortable range.

The proposed withdrawal mechanism of IACs is shown in Fig. 5. When the indoor temperature is within the comfortable range, switch S_1 keeps closed and switch S_2 keeps open. In this scenario, the control diagram of the IAC is the same with Fig. 4. In contrast, when the violation of the customer's temperature comfort requirement is detected, switch S_1 will be open and switch S_2 will be closed. It means that the consensus control output is disabled for this IAC while the frequency recovery output (f_i^0) is enabled. In other words, this IAC withdraws from the regulation process and returns to operate at the

initial operating frequency to guarantee the comfort. Take the upregulation scenario for example, the operating frequency f_i of the ith IAC is expressed as

$$f_i(t) = \begin{cases} f_i^0 - x_i(t) \cdot \left(f_i^0 - \underline{f_i}\right), & \text{Regulation status} \\ f_0^i \quad \forall i \in \mathcal{I} \quad \forall t \in \mathcal{T}, & \text{Withdrawal status.} \end{cases} \tag{18}$$

Note that the control modules of withdrawn IACs continue to communicate with neighbors using states x_i, even though these control modules no longer convert their output states x_i into the IACs' frequency control signals f_i. If these withdrawn IACs stop communicating with neighbors, some IACs may lose communication in the distributed consensus control framework and cannot provide operating reserve. After the withdrawal, the pseudo "state" of this specific IAC does not reflect the utilization level of the IAC's regulation capacity anymore. Instead, the pseudostate of the withdrawn IAC plays a role as intermediary for its neighbors. The proposed withdrawal mechanism can guarantee the customers' comfort requirements while not affecting the normal information exchange in the communication network.

E. Convergence Analysis of the Proposed Algorithm

The convergence of IACs' states is a major concern in the consensus algorithm with the nonlinear protocol, since it is directly related to the regulation objective. In this article, the Lyapunov stability theorem, as a powerful method in stability analysis of nonlinear systems, is utilized to prove the convergence [39].

Proof: All the states in the proposed consensus algorithm with the nonlinear protocol can converge to the decision value λ, i.e., $\boldsymbol{x} = \lambda\mathbf{1} = [\lambda, \ldots, \lambda]^T$. ■

Remark: It is assumed that the total number of nodes in the network is N. According to (14), the following property about the sum of $\dot{y}_i$ holds for the undirected graph:

$$\begin{aligned} \sum_{i=1}^{N} \dot{y}_i(t) &= \sum_{i=1}^{N} c \sum_{j \in \mathcal{N}_i} a_{ij}\big(x_j(t) - x_i(t)\big) \\ &= c \cdot \big[a_{ij}\big(x_j(t) - x_i(t)\big) + a_{ji}\big(x_i(t) - x_j(t)\big)\big] + \cdots \\ &\equiv 0 \quad \forall i \in \mathcal{I} \quad \forall t \in \mathcal{T}. \end{aligned} \tag{19}$$

Therefore, the sum $\sum_{i=1}^{N} y_i$ in the network remains invariant. It is an important and basic characteristic for the undirected graph (i.e., the network with bidirectional communication between neighbor nodes in this article). It essentially reflects the symmetry for interactions among IACs in the communication network. The sum of y_i [i.e., $\sum_{i=1}^{N} y_i(t)$] remains constant as the initial given value $\sum_{i=1}^{N} y_i(0)$ if there are no external interruptions.

According to different initial states, two scenarios can be analyzed separately.

Scenario 1 ($0 \le \sum_{i=1}^{N} y_i(0) \le N$): Let $\bar{y} = (1/N)\sum_{i=1}^{N} y_i(0)$, and the range of $\bar{y}$ satisfies $0 \le \bar{y} \le 1$ in the Scenario 1. Consider the following integral Lyapunov function [40]:

$$V = 2\sum_{i=1}^{N} \int_{\bar{y}}^{y_i} (\text{sat}(\omega) - \bar{y}) d\omega \quad \forall i \in \mathcal{I} \tag{20}$$

where $\text{sat}(\cdot)$ is a monotonically increasing function and $V \ge 0$ is satisfied. Furthermore, for the undirected graph $\mathcal{G}$, the Laplacian matrix $\boldsymbol{L}$ is symmetric with a trivial zero eigenvalue corresponding to the eigenvector $\mathbf{1}$. Therefore, $\bar{y}\mathbf{1}$ is the equilibrium point due to $\dot{\boldsymbol{y}} = -\boldsymbol{L}(\bar{y}\mathbf{1}) = -\bar{y}\boldsymbol{L}\mathbf{1} = \mathbf{0}$. Based on (20), $V = 0$ if and only if $\boldsymbol{y} = \bar{y}\mathbf{1} = \boldsymbol{x}$, i.e., $V = 0$ if and only if at the equilibrium point. Therefore, the basic requirement for the Lyapunov function is satisfied.

Since $(1/N)\sum_{i=1}^{N} \dot{y}_i \equiv 0$, the derivative of V can be obtained from (20) as follows:

$$\begin{aligned} \dot{V} &= 2\sum_{i=1}^{N} \text{sat}(y_i)\dot{y}_i - 2\bar{y}\sum_{i=1}^{N}\big(\dot{y}_i - \dot{\bar{y}}\big) \\ &= 2\sum_{i=1}^{N}\sum_{j=1}^{N} a_{ij} x_i\big(x_j - x_i\big) \quad \forall i \in \mathcal{I} \quad \forall j \in \mathcal{N}_i. \end{aligned} \tag{21}$$

Based on the following lemma for the undirected graph with $\forall a_i, b_i \in \mathbb{R}$ [41]:

$$\sum_{i=1}^{N}\sum_{j=1}^{N} a_{ij}\big(a_i - a_j\big)\big(b_i - b_j\big) = 2\sum_{i=1}^{N}\sum_{j=1}^{N} a_{ij} a_i\big(b_i - b_j\big) \tag{22}$$

the derivative $\dot{V}$ in (21) can be further transformed into:

$$\dot{V} = -\sum_{i=1}^{N}\sum_{j=1}^{N} a_{ij}\big(x_i - x_j\big)^2 \quad \forall i \in \mathcal{I} \quad \forall j \in \mathcal{N}_i. \tag{23}$$

Hence, $\dot{V} \le 0$ is always satisfied and the equilibrium point $\boldsymbol{y} = \bar{y}\mathbf{1}$ is Lyapunov stable. Furthermore, $\dot{V} = 0$ only when $x_i - x_j = \text{sat}(y_i) - \text{sat}(y_j) = 0$ in (23). According to the Lyapunov stability theorem, the asymptotic stability at the equilibrium point can be proved because $\dot{V} = 0$ only at the equilibrium point $\boldsymbol{y} = \bar{y}\mathbf{1}$.

Therefore, in Scenario 1, the equilibrium point $\boldsymbol{y} = \bar{y}\mathbf{1}$ is proved to be asymptotically stable. In other words, when $0 \le \sum_{i=1}^{N} y_i(0) \le N$, the consensus of IACs' states can be reached with the decision value $\lambda = \bar{y}$.

Scenario 2 ($\sum_{i=1}^{N} y_i(0) > N$ and $\sum_{i=1}^{N} y_i(0) < 0$): For $\sum_{i=1}^{N} y_i(0) > N$, none of the IACs can decrease the operating frequency anymore. Therefore, the consensus of x_i can be achieved as $\boldsymbol{x} = \mathbf{1}$, i.e., $\lambda = 1$.

For $\sum_{i=1}^{N} y_i(0) < 0$, none of the IACs can increase the operating frequency anymore. Therefore, the consensus of x_i can be achieved as $\boldsymbol{x} = \mathbf{0}$, i.e., $\lambda = 0$.

In summary, the consensus of $x_i = \text{sat}(y_i)$ in the network can be guaranteed under the application scenario of this article. It should be noted that there is a mismatch between the actual regulation capacity P_{DR} and the target regulation capacity P_{tgt}, when an IAC unit suddenly withdraws. It is equivalent to changing the initial condition for $\sum_{i=1}^{N} y_i(0)$, and a new converging process will begin at this moment. The proposed algorithm is designed to achieve the convergence of all states, including states of IACs that still provide operating reserve and pseudostates of withdrawn IACs. Therefore, the withdrawal of IACs will not influence the inherent convergence characteristics of the proposed algorithm.

TABLE I
PARAMETERS OF IACS AND CORRESPONDING ROOMS

Symbols	Parameters	Distributions[1]/Values	Units
l_{i1}	IAC operation coefficients	$\mathcal{U}$(0.0285,0.0315)	kW/Hz
b_{i1}	IAC operation coefficients	$\mathcal{U}$(-0.42,-0.38)	kW
l_{i2}	IAC operation coefficients	$\mathcal{U}$(0.057,0.063)	kW/Hz
b_{i2}	IAC operation coefficients	$\mathcal{U}$(-0.315,-0.285)	kW
$\underline{f_i}$	Lower limitation of IAC operating frequency	$\mathcal{U}$(15,30)	Hz
$\overline{f_i}$	Upper limitation of IAC operating frequency	$\mathcal{U}$(130,140)	Hz
R_i	Equivalent themal resistance	$\mathcal{U}$(1.9,2.1)	°C/kW
C_i	Equivalent air heat capacity	$\mathcal{N}$(390,78^2)	kJ/°C
$T^i_{\max}$	Upper bound of comfort range	$\mathcal{U}$(27,28)	°C
$T^i_{\min}$	Lower bound of comfort range	$\mathcal{U}$(20,23)	°C
T^i_{set0}	Initial indoor temperature	$\mathcal{U}$(23,26)	°C
T_o	Outdoor temperature	32	°C

[1] $\mathcal{U}$ denotes uniform distributions, and $\mathcal{N}$ denotes normal distributions.
[2] Uniform distributions of $T^i_{\max}$, $T^i_{\min}$ and T^i_{set0} are discrete with 0.5 °C as the interval.

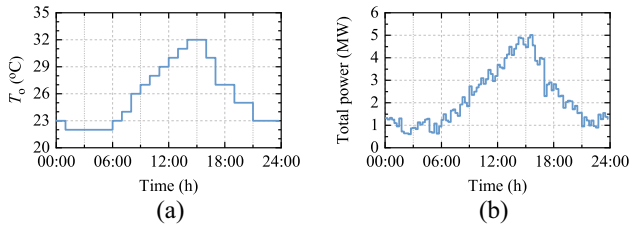

Fig. 6. Test scenario. (a) Outdoor temperature. (b) IACs' total operating power before regulation.

IV. CASE STUDIES

A. Test System

In this section, the proposed distributed consensus algorithm with the nonlinear protocol on large-scale IACs is verified by numerical studies. It is assumed that 3000 heterogeneous IACs in a community are controlled by an aggregator to provide operating reserve. The parameters of IACs and corresponding rooms' thermal characteristics are shown in Table I. The update of the IAC's state is conducted in a time-scheduled way and fixed at 1 s, which can well cover general short-distance wireless communication time and IAC's actuation time [35]. The control gain of IACs c is set as 0.15. The control coefficient of relay nodes β is set as 0.002. The outdoor temperature and IACs' total operating power before regulation in the test system are illustrated in Fig. 6. MATLAB R2016a is utilized as the simulation environment. The CPU model of the desktop for case studies is Intel Core i7-8700 and the frequency is 3.20 GHz.

It is assumed that a power dispatch signal is sent from the power system operator to the aggregator at 14:30 P.M. The signal includes the information of the specific regulation capacity (2 MW) and duration time (15 min). The aggregator is responsible for achieving the regulation requirement based on the proposed consensus algorithm with the nonlinear protocol.

B. Result Analysis of the Proposed Algorithm Performance

Fig. 7(a) shows the regulation process of the IACs' operating power under the upregulation scenario. It can be seen that

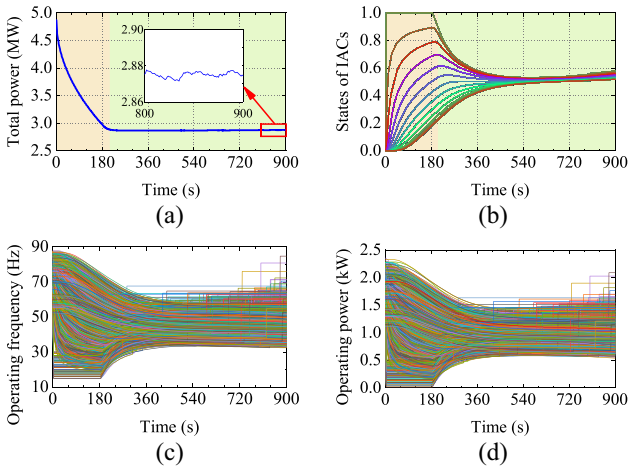

Fig. 7. Upregulation process of IACs for providing operating reserve with regulation capacity of 2 MW: (a) total operating power of IACs; (b) states of IACs; (c) operating frequency of IACs; and (d) operating power of IACs.

the required regulation capacity $P_{\text{tgt}} = 2$ MW is achieved in around the response time $T_R = 210$ s, which is fast enough for providing operating reserve. Therefore, the proposed distributed consensus algorithm can control IACs to realize the regulation capacity P_{tgt} with a short response time T_R. Besides, from the enlarged view in Fig. 7(a), the total operating power of IACs has small fluctuations during the regulation process. This is because the proposed withdrawal method can control IACs to stop providing operating reserve when their corresponding rooms' indoor temperatures reach the limitation. After that, the remaining IACs with available regulation capacity are controlled to compensate the lost regulation capacity of withdrawn IACs to maintain the required regulation capacity. The power fluctuations are around 0.01 MW, which is only 0.5% of the total regulation capacity. It can satisfy the power system's requirement of providing stable operating reserve within the duration time $T_D = 15$ min.

The dynamics of IACs' states are shown in Fig. 7(b). It can be seen that the consensus of IACs' states is achieved with the consideration of the nonlinear saturation effect. It verifies that the consensus algorithm is convergent even though we consider the IACs' physical constraints and application scenario requirements. According to the definition of IACs' states in (8), heterogeneous IACs can be regulated with similar utilization level of their power regulation potential. In addition, we find there is a slight rise of IACs' states after the consensus is achieved (e.g., time 720–900 s). This is because with the extension of regulation time, more IACs withdraw from the regulation due to the violation of customers' comfortable indoor temperature. In the meantime, the remaining IACs curtail more operating power to compensate the withdrawal effect, which leads to the slight rise of IACs' states. In any case, the consensus of IACs can always be achieved during the regulation process.

The operating frequency and power corresponding to the IACs' states are shown in Fig. 7(c) and (d), respectively. Apparently, all the IACs' operating frequency and power are decreased after the regulation signal. Some abruptly changing curves can be observed during the regulation process. This is

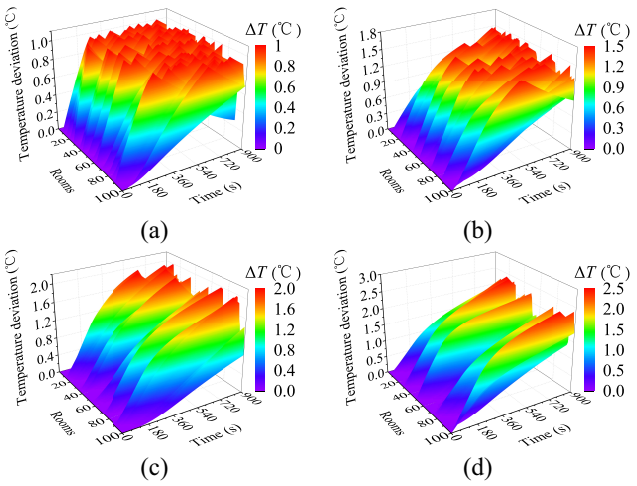

Fig. 8. Indoor temperature deviations during the upregulation process with regulation capacity of 2 MW under four allowable temperature deviations $\Delta T_{\max}$: (a) 1 °C; (b) 1.5 °C; (c) 2 °C; and (d) 2.5 °C.

because the operating frequencies of withdrawn IACs recover to the initial level according to the withdrawal mechanism. Compared with the state curves in Fig. 7(b), the corresponding operating frequency curve in Fig. 7(c) and operating power curve in Fig. 7(d) appear to be denser. This is because the heterogeneity of IACs' characteristics and their initial operating frequency are incorporated in the conversion based on the defined IACs' state values in (8).

C. Impact Analysis of Indoor Temperature

The indoor temperature deviations in different rooms are shown in Fig. 8 under the upregulation scenario. We randomly select 100 rooms for four scenarios with different allowable temperature deviation ranges, i.e., $\Delta T_{\max} = 1$ °C, 1.5 °C, 2 °C, and 2.5 °C, respectively. In Fig. 8(a), the indoor temperatures gradually rise as the IACs' operating power are decreased temporarily during the regulation process. When the indoor temperature of a specific room reaches the allowable temperature deviation of 1 °C, it can be detected by the control module and the withdrawal mechanism is activated immediately. The withdrawn IAC's operating frequency will recover to the initial level, so that the indoor temperature comfort of the customer can be guaranteed. With the increase of $\Delta T_{\max}$ from Fig. 8(a)–(d), the number of rooms that reach the allowable temperature deviation reduces, because larger allowable regulation range contributes to the continuous regulation. To sum up, the customers' comfort requirements with heterogeneous temperature sensitivities can always be guaranteed.

D. Result Analysis of Different Regulation Signals

For analyzing the impact of different regulation signals on IACs, four scenarios are assumed in this section under the upregulation scenario, where the regulation capacity is set as 1, 1.5, 2, and 2.5 MW, respectively. The response time T_R and the average of IACs' states $\boldsymbol{x}$ at the end of the regulation process are evaluated, as shown in Fig. 9. The average IAC state is used to reflect the overall utilization level of aggregated IACs' regulation capacity at the end of the regulation process.

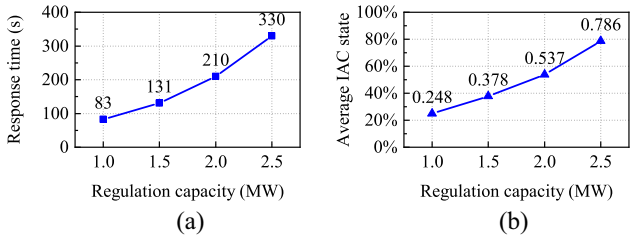

Fig. 9. System performance with different regulation capacity signals under the upregulation scenario: (a) response time and (b) average IAC state at the end of the regulation process.

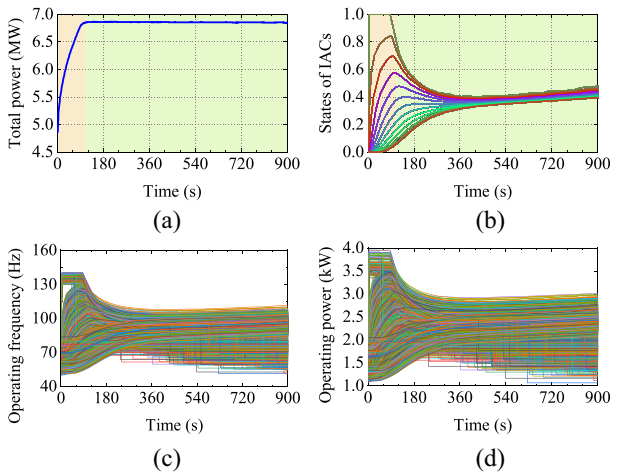

Fig. 10. Downregulation process of IACs for providing operating reserve with regulation capacity of 2 MW: (a) total operating power of IACs; (b) states of IACs; (c) operating frequency of IACs; and (d) operating power of IACs.

It can be seen from Fig. 9(a) that the response time T_R rises from 83 s in Scenario 1 to 330 s in Scenario 4 with the increase of the regulation capacity. All the response time in the four scenarios is less than 10 min and satisfy the system requirement for providing operating reserve.

It can be seen from Fig. 9(b) that the average of IACs' states $\boldsymbol{x}$ rises with a larger target regulation capacity P_{tgt}. In other words, IACs are adjusted with a smaller operating power to provide more operating reserve. Considering the maximum value of the IAC's state is 1, 100% of the regulation potential is utilized if the average of IACs' states $\boldsymbol{x}$ is equal to 1. In Scenario 1, about 24.8% of IACs' regulation potential is utilized averagely with the target regulation capacity $P_{\text{tgt}} = 1$ MW. The utilization level of IACs' regulation potential increases to about 78.6% averagely with the target regulation capacity $P_{\text{tgt}} = 2.5$ MW. Therefore, IACs are good flexible resources to provide adjustable operating reserve capacity based on the requirement of the power system operator.

E. More Result Analysis and Discussion

The control performance under the downregulation scenario with the regulation capacity of 2 MW is shown in Fig. 10. Compared to Fig. 7(a), Fig. 10(a) shows that aggregated IACs increase their total power consumption by 2 MW in about 120 s. Fig. 10(b) shows that the convergence of IACs' states under the downregulation scenario is also guaranteed. Fig. 10(c) and

(d) shows that IACs increase their operating frequency and operating power during the regulation process, respectively.

Moreover, compared with the simulation, the main difference of the implementation in the real world is the thermodynamic model of IACs. In the simulation, a classical dynamic model (1) is utilized to express the indoor temperature T_i deviations. In the real-world application, the dynamics of T_i may be much more complex. Parameters of rooms (e.g., C_i and R_i) may not be constants during the regulation process. The relationship between P_i/Q_i and f_i may not be ideally linear. Uncertain human behaviors (e.g., sudden opening of the door or window) may influence the dynamics of the indoor temperature. However, the above differences in the real-world application do not impact the applicability of the proposed method, because the withdrawal method is proposed based on the real-time monitored indoor temperature to ensure the temperature comfort of customers, regardless of the parameter uncertainties.

V. Conclusion

In this article, the distributed control of large-scale dispersed IACs for providing operating reserve was investigated. First, heterogeneous regulation capacities of IACs were normalized. On this basis, a distributed consensus algorithm with the nonlinear protocol was developed to control IACs for achieving the required regulation objectives, considering IAC physical constraints and the application scenario requirements. In addition, a withdrawal mechanism was proposed to terminate the regulation process of IACs violating temperature comfort requirements. The lost regulation capacity can be compensated by the remaining IACs still in the comfortable temperature ranges. Furthermore, based on the Lyapunov stability theorem, it is proved that the convergence of the proposed algorithm can always be guaranteed.

The feasibility and performance of the proposed distributed control method for IACs to provide operating reserve is verified by numerical studies. The results show that the control objectives can be successfully achieved, including the required regulation capacity, the response time and the duration time. Compared with previous studies, the proposed distributed consensus method features better data privacy protection, less communication and computation burden. It can provide useful reference for controlling IACs to provide operating reserve in the near future smart grid paradigm.

References

[1] "Renewable capacity statistics 2021," Int. Renew. Energy Agency, Abu Dhabi, UAE, Rep. 978-92-9260-342-7, 2021. [Online]. Available: https://www.irena.org/publications/2021/March/Renewable-Capacity-Statistics-2021

[2] Q. Shi, F. Li, G. Liu, D. Shi, Z. Yi, and Z. Wang, "Thermostatic load control for system frequency regulation considering daily demand profile and progressive recovery," *IEEE Trans. Smart Grid*, vol. 10, no. 6, pp. 6259–6270, Nov. 2019.

[3] H. Hui, Y. Ding, W. Liu, Y. Lin, and Y. Song, "Operating reserve evaluation of aggregated air conditioners," *Appl. Energy*, vol. 196, pp. 218–228, Jul. 2017.

[4] H. Liu, H. Xie, H. Luo, J. Qi, H. H. Goh, and S. Rahman, "Optimal strategy for participation of commercial HVAC systems in frequency regulation," *IEEE Internet Things J.*, vol. 8, no. 23, pp. 17100–17110, Dec. 2021.

[5] Y. Li, X. Cheng, Y. Cao, D. Wang, and L. Yang, "Smart choice for the smart grid: Narrowband Internet of Things (NB-IoT)," *IEEE Internet Things J.*, vol. 5, no. 3, pp. 1505–1515, Jun. 2018.

[6] H. Hui, Y. Ding, Q. Shi, F. Li, Y. Song, and J. Yan, "5G network-based Internet of Things for demand response in smart grid: A survey on application potential," *Appl. Energy*, vol. 257, Jan. 2020, Art. no. 113972.

[7] X. Zhang, M. Pipattanasomporn, T. Chen, and S. Rahman, "An IoT-based thermal model learning framework for smart buildings," *IEEE Internet Things J.*, vol. 7, no. 1, pp. 518–527, Jan. 2020.

[8] P. Yu, H. Hui, H. Zhang, G. Chen, and Y. Song, "District cooling system control for providing operating reserve based on safe deep reinforcement learning," Dec. 2021, *arXiv:2112.10949*.

[9] N. Mahdavi and J. H. Braslavsky, "Modelling and control of ensembles of variable-speed air conditioning loads for demand response," *IEEE Trans. Smart Grid*, vol. 11, no. 5, pp. 4249–4260, Sep. 2020.

[10] H. Hui, Y. Ding, and M. Zheng, "Equivalent modeling of inverter air conditioners for providing frequency regulation service," *IEEE Trans. Ind. Electron.*, vol. 66, no. 2, pp. 1413–1423, Feb. 2019.

[11] Y.-J. Kim, L. K. Norford, and J. L. Kirtley, "Modeling and analysis of a variable speed heat pump for frequency regulation through direct load control," *IEEE Trans. Power Syst.*, vol. 30, no. 1, pp. 397–408, Jan. 2015.

[12] "Green and efficient refrigeration action plan," Chin. Government, Beijing, China, Rep. 1054, 2019. [Online]. Available: http://www.gov.cn/xinwen/2019-06/15/5400474/files/3daad33b125443abbd88855b69c61d3c.pdf

[13] H. Hui *et al.*, "A transactive energy framework for inverter-based HVAC loads in a real-time local electricity market considering distributed energy resources," *IEEE Trans. Ind. Informat.*, early access, Feb. 9, 2022, doi: 10.1109/TII.2022.3149941.

[14] P. Siano and D. Sarno, "Assessing the benefits of residential demand response in a real time distribution energy market," *Appl. Energy*, vol. 161, pp. 533–551, Jan. 2016.

[15] Y. Chen, D. Qi, and C. Li, "Distributed dynamic averaging tracking without rate measurements," *IEEE Trans. Syst., Man, Cybern., Syst.*, vol. 51, no. 7, pp. 4359–4364, Jul. 2021.

[16] B. J. Kirby, "Spinning reserve from responsive loads," Oak Ridge Nat. Lab., Oak Ridge, TN, USA, Rep. ORNL/TM-2003/19, 2003. [Online]. Available: https://eta-internal-publications.lbl.gov/sites/default/files/spinning-reserves.pdf

[17] T. Jiang, P. Ju, C. Wang, H. Li, and J. Liu, "Coordinated control of air-conditioning loads for system frequency regulation," *IEEE Trans. Smart Grid*, vol. 12, no. 1, pp. 548–560, Jan. 2021.

[18] C. Huang, H. Zhang, Y. Song, L. Wang, T. Ahmad, and X. Luo, "Demand response for industrial micro-grid considering photovoltaic power uncertainty and battery operational cost," *IEEE Trans. Smart Grid*, vol. 12, no. 4, pp. 3043–3055, Jul. 2021.

[19] Y. Wu *et al.*, "Secrecy-based delay-aware computation offloading via mobile edge computing for Internet of Things," *IEEE Internet Things J.*, vol. 6, no. 3, pp. 4201–4213, Jun. 2019.

[20] M. Zeraati, M. E. H. Golshan, and J. M. Guerrero, "Distributed control of battery energy storage systems for voltage regulation in distribution networks with high PV penetration," *IEEE Trans. Smart Grid*, vol. 9, no. 4, pp. 3582–3593, Jul. 2018.

[21] Y. Ding, D. Xie, H. Hui, Y. Xu, and P. Siano, "Game-theoretic demand side management of thermostatically controlled loads for smoothing tie-line power of microgrids," *IEEE Trans. Power Syst.*, vol. 36, no. 5, pp. 4089–4101, Sep. 2021.

[22] Q. Zhou, M. Shahidehpour, A. Paaso, S. Bahramirad, A. Alabdulwahab, and A. Abusorrah, "Distributed control and communication strategies in networked microgrids," *IEEE Commun. Surveys Tuts.*, vol. 22, no. 4, pp. 2586–2633, 4th Quart., 2020.

[23] T. Chen *et al.*, "Optimal demand response strategy of commercial building-based virtual power plant using reinforcement learning," *IET Gener. Transm. Distrib.*, vol. 15, no. 16, pp. 2309–2318, Aug. 2021.

[24] Y. Wang, Q. Chen, C. Kang, and Q. Xia, "Clustering of electricity consumption behavior dynamics toward big data applications," *IEEE Trans. Smart Grid*, vol. 7, no. 5, pp. 2437–2447, Sep. 2016.

[25] R. Adhikari, M. Pipattanasomporn, and S. Rahman, "An algorithm for optimal management of aggregated HVAC power demand using smart thermostats," *Appl. Energy*, vol. 217, pp. 166–177, May 2018.

[26] Y. Wang *et al.*, "Aggregated energy storage for power system frequency control: A finite-time consensus approach," *IEEE Trans. Smart Grid*, vol. 10, no. 4, pp. 3675–3686, Jul. 2019.

[27] M. Shi, M. Shahidehpour, Q. Zhou, X. Chen, and J. Wen, "Optimal consensus-based event-triggered control strategy for resilient DC microgrids," *IEEE Trans. Power Syst.*, vol. 36, no. 3, pp. 1807–1818, May 2021.
[28] J. Qin, Q. Ma, Y. Shi, and L. Wang, "Recent advances in consensus of multi-agent systems: A brief survey," *IEEE Trans. Ind. Electron.*, vol. 64, no. 6, pp. 4972–4983, Jun. 2017.
[29] Y. Mo and R. M. Murray, "Privacy preserving average consensus," *IEEE Trans. Autom. Control*, vol. 62, no. 2, pp. 753–765, Feb. 2017.
[30] Y. Chen, C. L. D. Q. Z. Li, Z. Wang, and J. Zhang, "Distributed event-triggered secondary control for islanded microgrids with proper trigger condition checking period," *IEEE Trans. Smart Grid*, early access, Sep. 24, 2021, doi: 10.1109/TSG.2021.3115180.
[31] J. Fu, G. Wen, T. Huang, and Z. Duan, "Consensus of multi-agent systems with heterogeneous input saturation levels," *IEEE Trans. Circuits Syst. II, Exp. Briefs*, vol. 66, no. 6, pp. 1053–1057, Jun. 2019.
[32] S. Bhowmick and S. Panja, "Leader–follower bipartite consensus of linear multiagent systems over a signed directed graph," *IEEE Trans. Circuits Syst. II, Exp. Briefs*, vol. 66, no. 8, pp. 1436–1440, Aug. 2019.
[33] B. Wang, T. Zhang, X. Hu, Y. Bao, and H. Su, "Consensus control strategy of an inverter air conditioning group for renewable energy integration based on the demand response," *IET Renew. Power Gener.*, vol. 12, no. 14, pp. 1633–1639, Oct. 2018.
[34] H. Xing, Y. Mou, Z. Lin, and M. Fu, "Fast distributed power regulation method via networked thermostatically controlled loads," *IFAC Proc. Vol.*, vol. 47, no. 3, pp. 5439–5444, Aug. 2014.
[35] Y. Wang, Y. Tang, Y. Xu, and Y. Xu, "A distributed control scheme of thermostatically controlled loads for the building-microgrid community," *IEEE Trans. Sustain. Energy*, vol. 11, no. 1, pp. 350–360, Jan. 2020.
[36] N. Lu, "An evaluation of the HVAC load potential for providing load balancing service," *IEEE Trans. Smart Grid*, vol. 3, no. 3, pp. 1263–1270, Sep. 2012.
[37] M. Song, C. Gao, H. Yan, and J. Yang, "Thermal battery modeling of inverter air conditioning for demand response," *IEEE Trans. Smart Grid*, vol. 9, no. 6, pp. 5522–5534, Nov. 2018.
[38] R. Olfati-Saber, J. A. Fax, and R. M. Murray, "Consensus and cooperation in networked multi-agent systems," *Proc. IEEE*, vol. 95, no. 1, pp. 215–233, Jan. 2007.
[39] W. Brogan, *Modern Control Theory*, 3rd ed., Upper Saddle River, NJ, USA: Pearson, 1990.
[40] X. Liu, T. Chen, and W. Lu, "Consensus problem in directed networks of multi-agents via nonlinear protocols," *Phys. Lett. A*, vol. 373, no. 35, pp. 3122–3127, Aug. 2009.
[41] W. Ren, "On consensus algorithms for double-integrator dynamics," *IEEE Trans. Autom. Control*, vol. 53, no. 6, pp. 1503–1509, Jul. 2008.

Jiatu Hong (Student Member, IEEE) received the B.E. degree in electrical engineering from Dalian University of Technology, Dalian, China, in 2015, and the M.S. degree in power engineering from Queensland University of Technology, Brisbane, QLD, Australia, in 2018. He is currently pursuing the Ph.D. degree with the University of Macau, Macau, China.

His research interests include Internet of Things for smart energy and distributed control of flexible resources in smart grid.

Hongxun Hui (Member, IEEE) received the B.E. and Ph.D. degrees in electrical engineering from Zhejiang University, Hangzhou, China, in 2015 and 2020, respectively.

He is currently a Postdoctoral Fellow with the State Key Laboratory of Internet of Things for Smart City, University of Macau, Macau, China. From 2018 to 2019, he was a visiting student researcher with the Advanced Research Institute, Virginia Tech, Blacksburg, VA, USA, and the CURENT Center, University of Tennessee, Knoxville, TN, USA. His research interests include power system stability analysis, microgrid optimization, control of flexible resources, and Internet of Things technologies for smart energy.

Dr. Hui was elected in the 1st Batch of the Academic Rising Star Program for Ph.D. students in Zhejiang University in 2018.

Hongcai Zhang (Member, IEEE) received the B.S. and Ph.D. degrees in electrical engineering from Tsinghua University, Beijing, China, in 2013 and 2018, respectively.

He is currently an Assistant Professor with the State Key Laboratory of Internet of Things for Smart City and the Department of Electrical and Computer Engineering, University of Macau, Macau, China. From 2018 to 2019, he was a Postdoctoral Scholar with the Energy, Controls, and Applications Lab, University of California at Berkeley, Berkeley, CA, USA, where he also worked as a visiting student researcher in 2016. His current research interests include Internet of Things for smart energy, optimal operation and optimization of power and transportation systems, and grid integration of distributed energy resources.

Ningyi Dai (Senior Member, IEEE) received the B.Sc. degree in electrical engineering from Southeast University, Nanjing, China, in 2001, and the M.Sc. and Ph.D. degrees in electrical and electronics engineering from the Faculty of Science and Technology, University of Macau, Macau, China, in 2004 and 2007, respectively.

She is currently an Associate Professor with the Department of Electrical and Computer Engineering and the State Key Laboratory of Internet of Things for Smart City, University of Macau. She has authored or coauthored more than 70 technical journals and conference papers in power systems and power electronics. Her current research interests include application of power electronics in power systems, renewable energy integration, and integrated energy system.

Dr. Dai was a co-recipient of the Macao Science and Technology Invention Award in 2012 and 2018.

Yonghua Song (Fellow, IEEE) received the B.E. degree in electrical engineering from Chengdu University of Science and Technology, Chengdu, China, in 1984, the Ph.D. degree in electrical engineering from China Electric Power Research Institute, Beijing, China, in 1989, the D.Sc. degree from Brunel University London, Uxbridge, U.K., in 2002, the D.Eng. degree (Hons.) from the University of Bath, Bath, U.K., in 2014, and the D.Sc. degree (Hons.) from The University of Edinburgh, Edinburgh, U.K., in 2019.

From 1989 to 1991, he was a Postdoctoral Fellow with Tsinghua University, Beijing. He then held various positions with Bristol University, Bristol, U.K.; Bath University, Bath; and John Moores University, Liverpool, U.K., from 1991 to 1996. In 1997, he was a Professor of Power Systems with Brunel University London, where he has been a Pro-Vice Chancellor for Graduate Studies since 2004. In 2007, he took up a Pro-Vice Chancellorship and the Professorship of Electrical Engineering with the University of Liverpool, Liverpool. In 2009, he joined Tsinghua University as a Professor of Electrical Engineering and an Assistant President and the Deputy Director of the Laboratory of Low-Carbon Energy. From 2012 to 2017, he worked as the Executive Vice President of Zhejiang University, Hangzhou, China, as well as the Founding Dean of the International Campus and the Professor of Electrical Engineering and Higher Education of the University. Since 2018, he has been a Rector of the University of Macau, Macau, China, and the Director of the State Key Laboratory of Internet of Things for Smart City. His current research interests include smart grid, electricity economics, and operation and control of power systems.

Prof. Song was elected as the Vice-President of the Chinese Society for Electrical Engineering (CSEE) and appointed as the Chairman of the International Affairs Committee of CSEE in 2009. In 2004, he was elected as a Fellow of the Royal Academy of Engineering, U.K. In 2019, he was elected as a Foreign Member of the Academia Europaea.